Near-threshold displacements in tantalum single crystals

M. Biget, F. Maury, P. Vajda, A. Lucasson,* and P. Lucasson
Equipe de Recherches du Centre National de la Recherche Scientifique, Laboratoire de Chimie Physique, Bâtiment 350, F-91405 Orsay, France
(Received 22 July 1977)

Tantalum single crystals of the four orientations (100), (110), (111), and (112) have been irradiated with electrons in the energy range 1.0–1.7 MeV. A special irradiation procedure has been used which enables us to distinguish between subthreshold and intrinsic defects. The threshold energy for atomic displacement is found to be the lowest in and around the ⟨100⟩ direction. Moreover, the defect production in the ⟨100⟩ direction is found to be governed by two slightly different threshold energies. An analysis based on a geometrical model for the threshold energy surface leads to the following results: $T_{d1}^{\langle 100\rangle} = 33 \pm 1$ eV, $T_{d2}^{\langle 100\rangle} = 38 \pm 1$ eV, and $T_d \geq 55$ eV for all other crystallographic directions. Although several models can account for the observed defect production rates, these two different values for the threshold energy in the ⟨100⟩ direction can best be interpreted as corresponding to different separation distances between the interstitial atom and its vacancy; for the closest distance, i.e., the lowest threshold energy, only one of the two possible configurations of the Frenkel pair (depending on the orientation of the split interstitial with respect to the pair axis) is stable at the irradiation temperature. A value of $\rho_F^{Ta} = 16 \pm 3$ $\mu\Omega$ cm per at.% is deduced for the Frenkel-pair resistivity in tantalum. An empirical interatomic potential of a Born-Mayer form is proposed in the range $1.4 < r < 2.7$ Å. Finally, a tentative interpretation is given for the tantalum recovery spectrum between 7 and 20 K.

I. INTRODUCTION

When, a few years ago, Jung and Schilling[1] published their results of an irradiation of tantalum crystals with electrons in the energy range 1.0 to 3.2 MeV, the conclusions to be drawn from these data caused some surprise. In fact, they had determined the threshold energy surface for atomic displacement throughout the fundamental triangle and found that good overall fits were only possible when the average threshold was ~36 eV in a region of 20° around the ⟨111⟩ direction, ~53 eV in a region of 18° around the ⟨100⟩ direction, and larger than 130 eV in other directions. (The lowest threshold energy was found to be 32 ± 2 eV.) This was in contrast with the only other data existing at the time for a bcc metal, α-iron. In the latter case, both computer simulations[2] and direct irradiation experiments[3] had clearly indicated that the lowest-threshold-energy region was near the most open ⟨100⟩ direction. Jung and Schilling argued that the computer findings might be the result of a bad choice as concerns the interaction potential used for the simulation. The contradiction remained open.

In the meantime, more experiments were performed on bcc crystals, and their analyses pointed always in favor of the original conclusions on α-iron rather than in favor of the tantalum results of Jung and Schilling. Thus, in an extensive study[4,5] of molybdenum crystals electron irradiated along different directions, the lowest threshold has been observed in the ⟨100⟩ direction, while $T_d^{\langle 111\rangle}$ was about 30% higher than $T_d^{\langle 100\rangle}$. A detailed work on α-iron[6] completing the pioneering experiments of Lomer and Pepper[3] confirmed their results, again yielding a minimum T_d in the ⟨100⟩ direction. Further indications can be drawn from a study done by Dausinger[7] who investigated the recovery of tungsten crystals irradiated with 3-MeV electrons. The defect production rate at this energy, corresponding to roughly $3T_d^{min}$ (T_d^{min} is the minimum threshold energy), was lowest for the (100) crystal, followed by the (111) and the (110) crystals quite in analogy to molybdenum and α-iron, while the damage rate of the tantalum crystals at the corresponding transmitted energy was lowest for the (111) samples followed by (110) and (100). The situation has been resumed in a review article by one of the present authors.[8]

Since the knowledge of the threshold energy surface is very important in view of the possible deduction of fundamental quantities such as Frenkel-pair resistivities and interaction potentials in a metal (see, e.g., Ref. 8 and references therein), we decided to repeat Jung and Schilling's experiment. We proceeded to irradiate tantalum crystals of various orientations looking especially for details close to the threshold, since the analysis of the observed anisotropy is clearest in this region as shall be shown in the paper. At the same time, we have looked for anisotropy manifestations in the annealing spectrum at low temperatures.

In the following, we are presenting the results of an electron-irradiation experiment at liquid-

helium temperatures, an analysis of the data taking into account the production of subthreshold defects, together with a discussion concerning the discrepancy with the Jung-Schilling experiment and the possible displacement mechanisms at low energies.

II. EXPERIMENTAL DETAILS

The specimens were prepared from monocrystalline tantalum rods grown by the Ecole des Mines de St. Etienne. The rod axis had been chosen parallel to the ⟨110⟩ direction so that all the principal crystallographic planes could be obtained by simple rotation around this axis. The orientation by Laue x-ray radiography and the cutting of platelets parallel to the (100), (110), (111), and (112) planes were performed by means of a goniometric adaptor especially constructed for this purpose.[9] After mechanical polishing down to ~150μ, cutting into strips and chemical polishing[10] in a solution of 50-ml H_2SO_4 + 20-ml HNO_3 + 20-ml HF, the final specimen dimensions were 25×0.5 mm^2, with thicknesses varying between 10 and 20 μ uniform to ± 3 μ. Before polishing, the strips had been annealed by Joule heating in a vacuum of $<10^{-7}$ Torr for 8 h at 2500–3000 °C. The quality of the irradiated samples was checked by measuring the electrical resistivity ratio, $\mathcal{R} = \rho_{300}/\rho_{4.2K}$; the rather low values found indicated a high residual impurity concentration. Mass-spectrometric and chemical analyses have shown an important concentration of hydrogen and of oxygen (cf. Table I). Backscattering analysis indicated for the irradiated specimens a higher oxygen content than given in Table I, which could—at least partially—imply an oxide layer on the surface. Table II summarizes the characteristics of the irradiated specimens.

For the electrical measurements, the samples have been provided with copper contacts in form of sandwiches spot welded onto the foil ends and then covered with soft solder. The latter becoming superconducting below ~7 K this eliminates any possible contribution of the contact material.

For irradiation and measurement purposes, the samples were placed in a liquid-helium cryostat[11] modified so as to include a superconducting magnet. This magnet provides a field necessary to suppress the superconductivity of the tantalum specimens. Their transition temperature $T_c = 4.5$ K is close enough to the measuring temperature of 4.2 K (chosen for its stability and reproducibility), so that a field of ~1 kOe was sufficient to render the foils normal (but not the solder). The irradiation was performed using electrons in the energy range 1.0 to 1.7 MeV extracted from a Cockroft-Walton vertical accelerator. The irradiation temperature was $\lesssim 7$ K monitored by the electrical resistivity of the irradiated specimens themselves, in addition to the traditional platinum and carbon resistors. The beam uniformity was assured by a beam sweep system and by a scattering foil placed in the beam tube roughly 1 m above the sample chamber. The annealing studies were made *in situ*, heating the entire sample chamber in 10-min pulses. The damage introduced by the electrons and its recovery were determined by measuring the variations of the electrical resistivity of the specimens at 4.2 K. The measuring sensitivity was 1×10^{-11} Ω cm.

TABLE I. Chemical sample analysis after mechanical and short chemical polishing.

Orientation	Hydrogen concentration	Oxygen concentration
(100)	143 ± 14 ppm	35 ± 5 ppm
(110)	•••	44 ± 5 ppm
(111)	120 ± 12 ppm	23 ± 5 ppm

III. EXPERIMENTAL DATA

A. Preliminary experiments

1. Damage rate at low energies, subthreshold defects

Tantalum has been shown[12,13] to exhibit important subthreshold effects which are likely to be related to the presence of gas impurities. Eliminating them is essential to obtaining some information on the properties (here, the threshold energies) of the intrinsic defects. This task, however, is not easy to achieve, especially in the case of

TABLE II. Characteristics of the irradiated samples.

Sample	(100)-*a*	(100)-*b*	(112)	(110)	(111)-*a*	(111)-*b*
$\rho_{295}/\rho_{4.2K}$	60	19	105	45	53	20
Mean thickness in μ	20	20	9	20	22	18

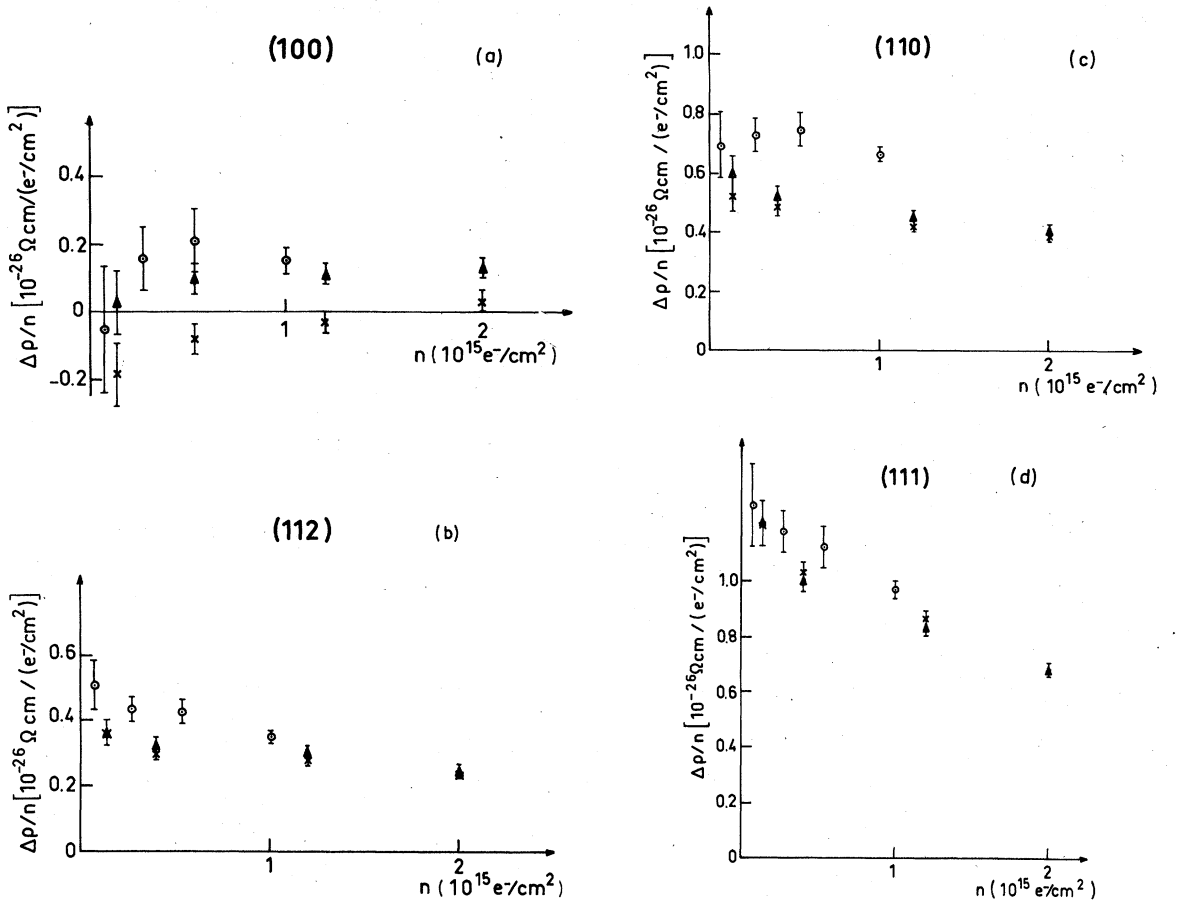

FIG. 1. Induced-resistivity change rates as a function of the incident electron fluence for three runs (i) at 1.0 MeV: ⊙, (ii) second run at 1.0 MeV: ×, (iii) at 1.3 MeV: ▲, for four orientations: (100)—curve (a), (112)—curve (b), (110)—curve (c), (111)—curve (d).

samples like ours, which contain non-negligible amounts of hydrogen and oxygen. A series of preliminary experiments was performed as an attempt to master the production of subthreshold defects and possibly subtract them from the total damage production.

The six samples described in Table II were irradiated at a fixed energy chosen successively below, near, and above the supposed threshold, and the damage production rate was measured as a function of the incident electron fluence. The first two irradiations were performed on two following days (the samples were annealed during the night inbetween up to 160 K) at the same energy, 1.0 MeV, which is below threshold. A third irradiation was performed a few days later at 1.3 MeV, which is assumed to be slightly above threshold[1] and a fourth one on the following day, at 1.7 MeV, which is well above threshold. Figures 1(a)–1(d) show the measured damage rate as a function of the incident electron fluence for the four samples (100)-*a*, (112), (110), and (111)-*a* during the first three irradiations—at 1.0, 1.0, and 1.3 MeV. The error bars take into account the dispersion of the electrical measurements and the possible changes in the beam profile during the same day. Several facts are to be pointed out. (a) The subthreshold production rate (production rate at 1.0 MeV) is large and saturates rapidly. Similar values (both for the production rate at the origin as well as for its rate of decrease with increasing fluence) have been measured in the case of polycrystalline cadmium.[14] An explanation has been given in terms of "hydrogen detrapping," involving the role played by the secondary electrons, which holds here as well. (b) The subthreshold production rate depends much on the sample orientation; it is not directly related to the resistivity ratio (see Table II) since the production rates for samples (100)-*b* and (111)-*b* (which are not shown here) are similar to those of samples (100)-*a* and (111)-*a*, respectively, al-

though their resistivity ratios are much smaller. A similar behavior (subthreshold effects strongly dependent on sample orientation) has been observed for high-purity monocrystals of cadmium.[15] As long as systematic studies in the field have not yet been done, this orientation dependence remains unexplained. (c) The subthreshold production rate is not reproducible from one day to another. This is most visible for the (100) and the (110) samples.

A possible explanation of the subthreshold production rate is the following: during the cooling of the sample, part of the interstitial hydrogen atoms is transformed from α phase into tantalum hydride, as shown in Ref. 16, the hydride concentration depending on the cooling conditions. The subthreshold resistivity increase would then correspond to the radiation induced dissociation of the hydride. Similar effects have been observed in experiments[17] with the system lutetium-hydrogen in the α-phase range, which exhibited strong resistivity increases when irradiated below the lutetium threshold (~0.8 MeV) at low temperatures.

Moreover, the results of Meissner[12] and Faber[13] on polycrystalline tantalum have shown that the subthreshold production rate was not a simple function of the doped-in impurity concentration, neither with regard to oxygen nor to hydrogen. The recent study of Rosan and Wipf[16] demonstrates that the presence of nitrogen traps suppresses strongly the formation of hydride precipitates. All this proves the complexity of gas impurity behavior in tantalum and, consequently, that of subthreshold defect production which appears to be related to the former one.

2. Recovery

Isochronal anneals were performed after each irradiation. The results are summarized in Table III. They are given in absolute values for the same irradiation dose: $n = 10^{15}$ electrons/cm^2, and will be discussed in Sec. IV D. We will just note here that an important recovery takes place between 40 and 60 K; its amplitude after the 1.0- and the 1.3-MeV irradiations reaches more than 100% of the total induced resistivity. Furthermore, a subsequent anneal was performed at 120 K which led to an increase of the resistivity. These results are similar to those obtained by Schweikhardt[18] after quenching tantalum specimens containing 200 at. ppm of hydrogen in the α phase.

3. Conclusion

Due to the nonreproducibility discussed above, nothing can be said from these results on the production of intrinsic defects at 1.3 MeV, although a definite difference is observed for the (100) sample between the production rates at 1.0 MeV (second irradiation) and 1.3 MeV (third irradiation), cf. Fig. 1a. A similar difference does not appear for the three other irradiated orientations.

B. Results

1. Irradiating procedure

In order to eliminate the difficulty arising from the possible nonreproducibility of the subthreshold effects, the samples were irradiated alternately (and repeatedly) below and above threshold. The value of 1.0 MeV was chosen as the energy of the subthreshold reference irradiations. Figures 2(a) to 2(d) present, as an example, the results obtained for the two energies 1.4 and 1.6 MeV. For each orientation, the production rates are plotted as a function of the total dose. We shall assume that the production rates of the intrinsic defects are given by the differences between the production rates below and above threshold taken at a same dose. One can see from the curves of Figs. 2 that the four samples behave in a very different way at 1.4 MeV. The intrinsic defect production rate, according to our definition, decreases markedly and steadily from the (100) to the (111) orientation.

TABLE III. Resistivity changes (units of 10^{-9} Ω cm) produced by irradiation and by subsequent annealing.

	(100) $\Delta\rho_{ann} \pm 0.05$				(112) $\Delta\rho_{ann} \pm 0.02$				(110) $\Delta\rho_{ann} \pm 0.03$				(111) $\Delta\rho_{ann} \pm 0.04$			
E	$\Delta\rho_{irr}$	T_{ann}			$\Delta\rho_{irr}$	T_{ann}			$\Delta\rho_{irr}$	T_{ann}			$\Delta\rho_{irr}$	T_{ann}		
(MeV)	±0.05	21 K	35 K	60 K	±0.02	21 K	35 K	60 K	±0.03	21 K	35 K	60 K	±0.04	21 K	35 K	60 K
1.0	−0.11				0.33	0.02	0.05	0.43	0.51	0.04	0.09	0.79	1.11	0.04	0.11	1.24
1.3	0.09	0.01	0.03	0.19	0.36	0.02	0.05	0.43	0.56	0.03	0.09	0.74	1.11	0.05	0.12	1.19
1.7	1.14	0.10	0.16	0.82	1.69	0.05	0.14	1.01	1.48	0.14	0.25	1.32	2.10	0.09	0.22	1.70

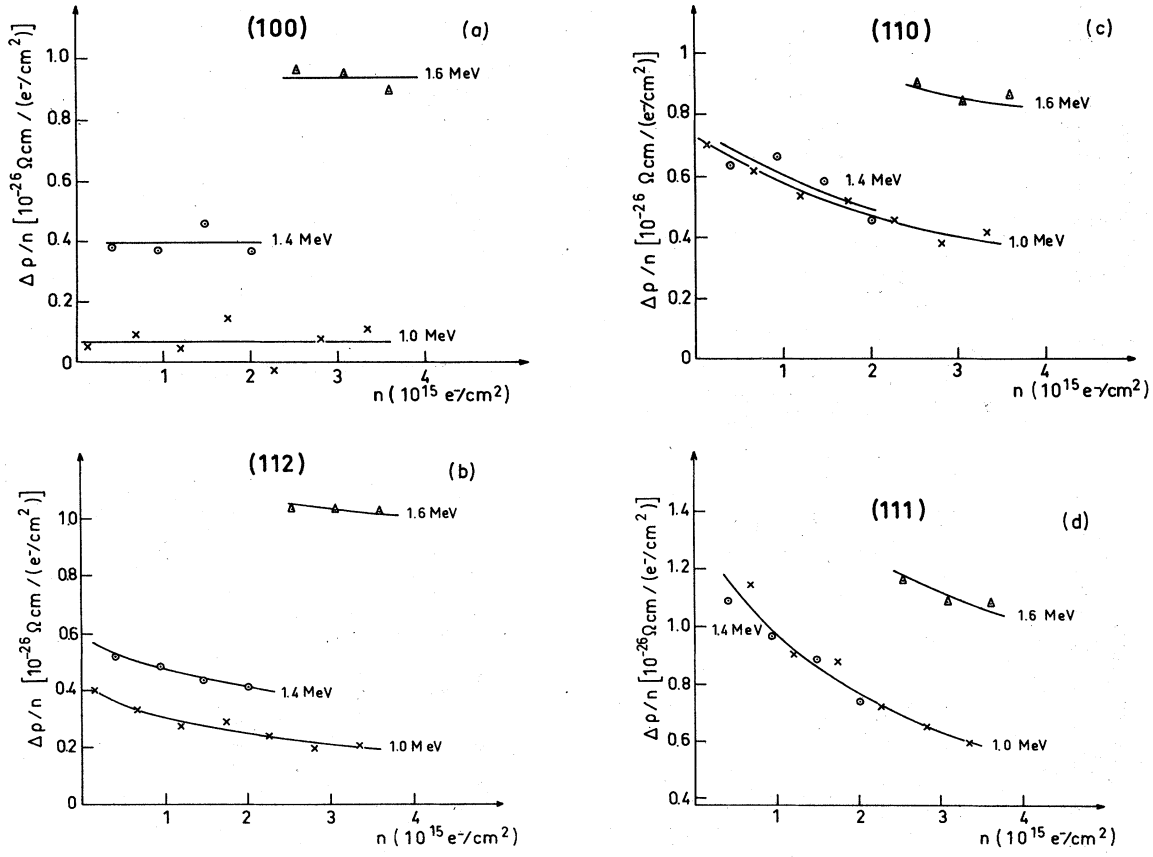

FIG. 2. Induced resistivity change rates as a function of the incident electron fluence in alternate irradiations below and above threshold for four orientations: (100)—curve (a); (112)—curve (b); (110)—curve (c); (111)—curve (d). The solid lines are eye fits through the experimental points.

2. *Production curves*

The measured production rates, as a function of energy, are displayed in Figs. 3(a)–3(d). The error bars correspond to the standard deviations calculated from the experimental points of Fig. 2. The curves drawn through the points are eye fits. The same curves are shown together on Fig. 3(e), so as to allow a quick comparison between the four orientations. The accuracy was best for the (112) sample (the thinnest one). Two points are to be noted. (i) The threshold energy appears to be minimum in the ⟨100⟩ direction, in agreement with other bcc metals[3,4,6] as well as with computer results,[2] and in contradiction to Jung and Schilling's results.[1] In fact, the disagreement with the latter concerns not only the lowest threshold energy but the whole shape of the production curves between 1.3 and 1.7 MeV for the (100) and the (111) orientations. As a possible explanation for this discrepancy, we suggest that Jung's samples could have been misoriented. This assumption is supported by a careful examination of the Laue x-ray diagrams presented by Jung in Ref. 19. (Actually, qualitative agreement is obtained between Jung's and our experimental curves when permuting his sample orientations so as to correct for possible misalignment: essentially ⟨100⟩ ⇄ ⟨111⟩.) (ii) Another observation results from Fig. 3. The next-lowest threshold displacement mechanism appears to take place also in the ⟨100⟩ direction. This follows from the occurrence of a large increase in the production rate between 1.35 and 1.4 MeV for the (100) sample, while, at the same energies, the production rates for the three other orientations remain smaller and only slightly increasing. The question arises then as to whether this part of the production curve which lies between 1.25 and 1.35 MeV for the (100) orientation corresponds to real intrinsic defects. A contribution from metallic impurities can be excluded since the involved concentrations would have to be much too high in order to get an effect of the observed amplitude. Even a mechanism where unstable Frenkel

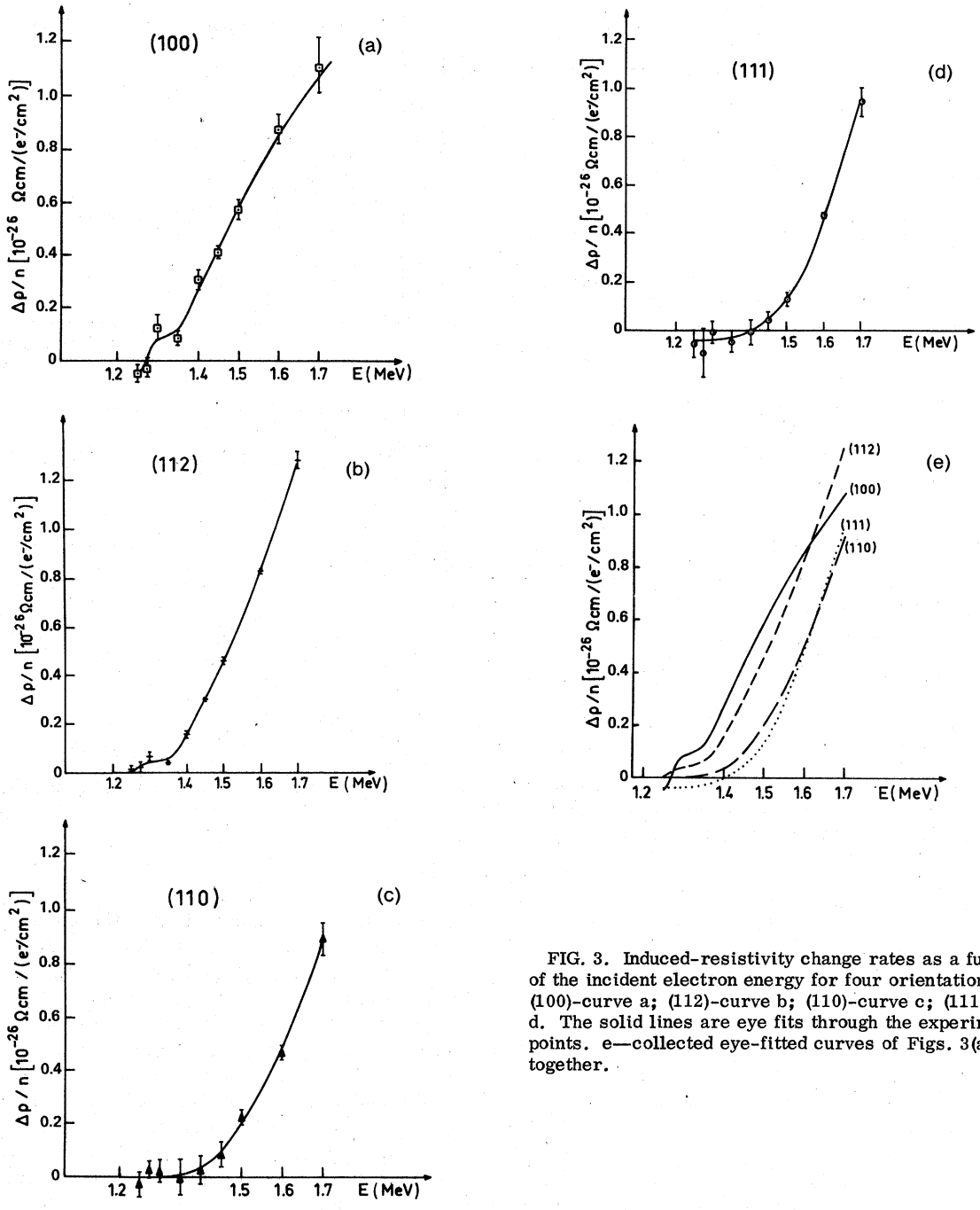

FIG. 3. Induced-resistivity change rates as a function of the incident electron energy for four orientations: (100)-curve a; (112)-curve b; (110)-curve c; (111)-curve d. The solid lines are eye fits through the experimental points. e—collected eye-fitted curves of Figs. 3(a)–3(d) together.

pairs, formed by replacement collisions, would be stabilized by the presence of gaseous or metallic impurities along the collision chain cannot account for the measured production rate unless the impurity concentration is as high as 1 at.%.

Let us now examine the hypothesis on which our subtraction of subthreshold effects is based and their possible implications.

3. *Discussion of the experimental procedure*

It has been assumed that the production rate of the subthreshold events does not depend on the bombarding energy in the range 1.0 to 1.7 MeV. In fact, if the subthreshold defects were to be attributed to the displacement of light impurities with very low threshold energies, the correspond-

ing production rate could decrease slightly with energy. The model developed in Ref. 14 gives a decrease of 10% between 0.8 and 1.7 MeV. Moreover, if the subthreshold defects were to be associated with propagation of focusons over long distances, their production rate should decrease with energy as the length of the collision chains. The zero intrinsic production rate observed, for example, at 1.4 MeV on Fig. 2(d) [(111) sample] would then result from a cancellation between a nonzero intrinsic production rate and a reduction of the subthreshold production rate between 1.0 and 1.4 MeV. This would explain the negative production rates observed below 1.4 MeV. However, the (112) sample, for which the measurements are the most accurate ones, does not exhibit any negative production rate. In order to illustrate the correctness of the hypothesis according to which the subthreshold production rate does not depend much on the energy, all points taken at various subthreshold energies for the (111) sample have been plotted in Fig. 4 as a function of the electron fluence only, not taking into account the different energies of other points taken in between. All these points lie roughly on the same curve. (Let us note that the obtained values are quite comparable to those given by Jung in Fig. 23 of Ref. 19.) If, nevertheless, the subthreshold production rate were a slightly decreasing function of the incident energy, the production curves would have to be shifted towards the positive production rates by an amount which would slowly increase with energy. This correction would not change the major features of the curves and, in particular, would be unable to account for the observed structure at low energies.

We have neglected the recombination of the close Frenkel pairs produced at an energy above threshold by the subsequent subthreshold irradiation. The recombination, proportional to the initial Frenkel-pair concentration, can be estimated from Meissner's results.[12] Each subthreshold irradiation (corresponding to a dose of 2.7×10^{14} electrons/cm^2) is found to induce the recombination of 3.5×10^{-6} of the already present Frenkel pairs. This is quite negligible due to the very low concentrations at which we are working.

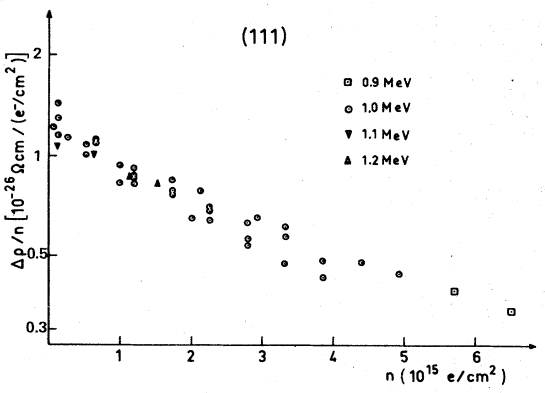

FIG. 4. Resistivity change rates as a function of incident electron fluence for the (111) crystal at various subthreshold energies.

4. Conclusion

A visual extrapolation without corrections [such as the one drawn in Fig. 3(a)] gives a threshold energy of 34 eV for the lowest threshold and ~38 eV for the second one. The lower value, 34 eV, is comparable to the value 32 ± 2 eV obtained by Youngblood *et al.*[20] with well outgassed samples (the damage production curves being linear with the electron fluence) at an irradiation temperature of 23 K. This supports the assumption we shall make in interpreting the experimental results, i.e., the structure which appears below 1.35 MeV in the (100) and (112) production curves is not an artifact but corresponds to real intrinsic defects. We have already noted in Ref. 6 that in the cases of both Fe and Mo, the (100) experimental production curves exhibited a bump at $T\sim1.3T_d^{\min}$, which was never reproduced by the calculations. This bump may be compared (although it is of less importance) to the structure observed for tantalum.

IV. DISCUSSION

A. Determination of the threshold energies

The analysis of the results is made on the basis of a geometrical model for the threshold energy surface of a bcc lattice. The calculational method has been described in detail in Ref. 5. The corrections for beam dispersion and energy losses are treated as in Ref. 6; losses due to radiation, which are not negligible in the case of high atomic numbers (for tantalum, $Z=73$), have been taken into account in addition to ionization losses. The Mott scattering cross sections have been obtained from the tables given by Oen in Ref. 21.

The geometrical model already used for molybdenum and iron[5,6] is unable to provide a fit of the experimental results in the case of tantalum, since it assumes the threshold energy in and around the ⟨100⟩ direction to be unique. Two models will be presented in the following, both giving satisfactory agreement with the experimental production curves.

1. Model I

The region of low threshold energy around the ⟨100⟩ direction was divided into two concentric

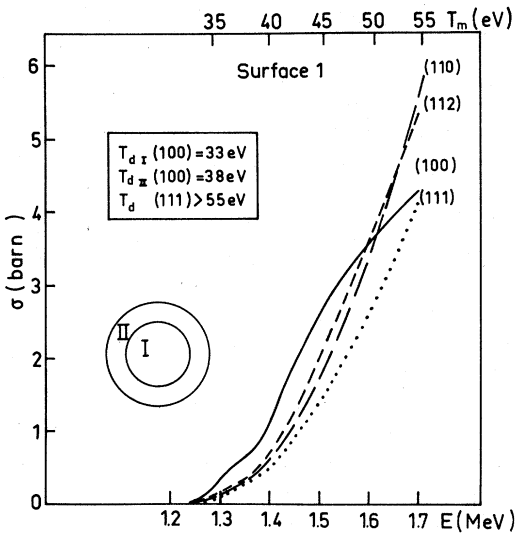

FIG. 5. Displacement cross sections calculated with model I.

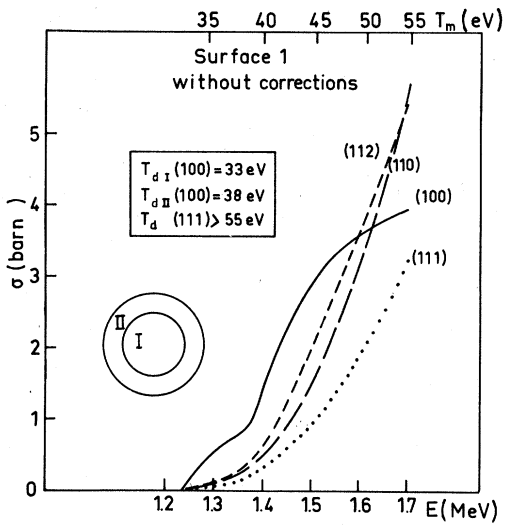

FIG. 7. Displacement cross sections calculated without corrections for energy loss and beam straggling.

regions of different threshold energies, the inner part of the lens being called region I, the annular part around it region II. The dimensions as well as the corresponding energies of these two regions were treated as parameters and determined to give the best fit with the experimental points of Fig. 3 taking into account the size of the error bars. This best fit (shown in Fig. 5) was obtained with $T_{dI}^{\langle 100\rangle} = 33$ eV, $T_{d\,II}^{\langle 100\rangle} = 38$ eV, and $T_d \gtrsim 55$ eV for all other directions. The maximum opening was 12° for region I and 20° for region II. The amplitude of the production cross section below 1.4 MeV is governed by the opening of region 1. Figure 6 illustrates the reduction of the cross section due to a reduction of region I from 12 to 10 degrees, the total opening of regions I+II being constant. The influence of the corrections for dispersion and energy losses is shown on Fig. 7, where the different curves have been calculated without corrections and which is to be compared with Fig. 5; the fit is somewhat better at lower energies and worse at the higher ones. A notable difference between Figs. 5 and 7 is observed, e.g., in the shape of the (100) curve, at higher energies; this prevents any accurate determination of threshold energies corresponding to other crystallographic directions, which would lie above 1.6 MeV, i.e., above ~50 eV.

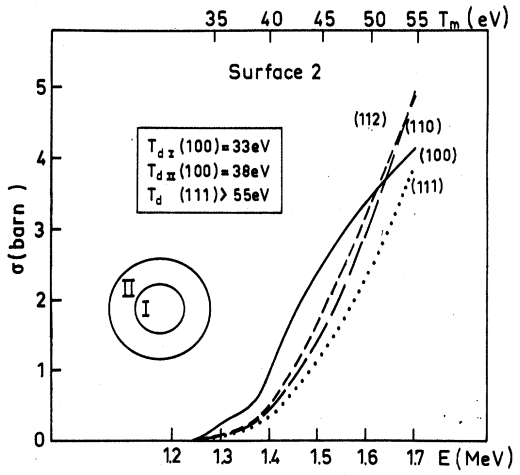

FIG. 6: Displacement cross sections calculated with model I using a modified threshold energy surface.

It must be noted that fitting the experimental results at low energies requires a very sharp increase in the threshold energy from region I to region II and not a continuous increase when going off the ⟨100⟩ direction. This discontinuity implies that two different mechanisms should be associated with the two regions. Region I could correspond to assisted focusing (along the ⟨100⟩ direction) although the crystal geometry does not favour this process. Yet, even with this hypothesis, the sharp delimitation between the two regions is still difficult to explain, so that the model does not seem to have much physical support.

2. *Model II*

It has been shown in the case of molybdenum[22] that the Frenkel pairs created in the ⟨100⟩ direction (in and around, i.e., in a solid angle of about the same opening—here 20°—as those used for molybdenum,[5] iron,[6] and by Jung[1] for tantalum) possess two different configurations depending on the orientation of the split-interstitial axis

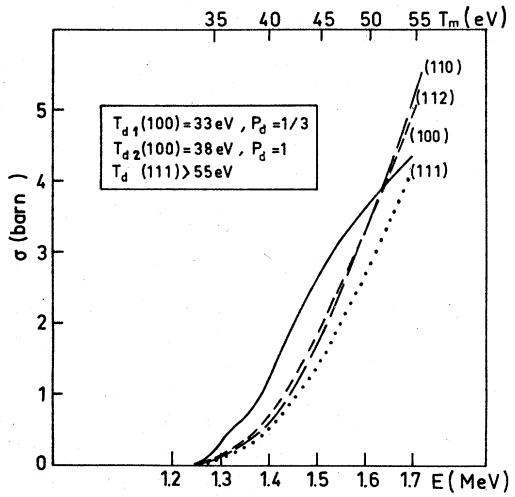

FIG. 8. Displacement cross sections calculated with model II.

with respect to the ⟨100⟩ direction. It is assumed in model II that for the minimum separation distance between the vacancy and the interstitial (corresponding to the minimum threshold energy $T_{d1}^{\langle 100\rangle}$), only one of these pairs—i.e., a certain fraction P_d of the created defects—is stable. For greater separations (corresponding to transmitted energies $\gtrsim T_{d2}^{\langle 100\rangle}$), both kinds of pairs are stable. Figure 8 shows that the best fit obtained with $T_{d1}^{\langle 100\rangle} = 33$ eV, $P_d = \frac{1}{3}$, $T_{d2}^{\langle 100\rangle} = 38$ eV and $T_d \gtrsim 55$ eV for all other directions. The value $\frac{1}{3}$ obtained for the parameter P_d means that one third only of the Frenkel pairs created in the ⟨100⟩ direction with the minimum separation distance, i.e., with a transmitted energy lying between 33 and 38 eV, are stable.

B. Determination of the Frenkel-pair resistivity

The Frenkel-pair resistivity ρ_F is deduced from the measured production rates and the calculated displacement cross sections σ according to the relation $\Delta\rho/n = \sigma\rho_F$. With both models, it is found: $\rho_F = 16 \pm 3$ μΩcm/at.% Frenkel pairs. This value depends mainly on the total opening (taken to be 20° according to Erginsoy's calculation) of the (100) lens. It is quite comparable to Jung's value, 17 ± 3 μΩcm/at.%, and in perfect agreement with the empirical rule,[23] ρ_F/at.% = $0.15\rho(T_m)$, where T_m is the melting point, giving also 16 μΩcm/at.%.

C. Determination of an interatomic potential

An empirical potential given in a Born-Mayer form, $V(r) = Ae^{-br}$, is deduced from the preceding determination of the displacement thresholds in the main crystallographic directions by calculating the energies needed to penetrate the various potential barriers in these directions. The details of the calculation are exposed in Refs. 5 and 24. The validity range of the obtained potentials goes from $a_0/2$ to $0.9a_0$, where $a_0 = 2.86$ Å is the nearest-neighbor distance.

The condition $T_d^{\langle 100\rangle} = 33$ eV leads to the determination of one of the two parameters A and b of the potential as a function of the other. The relation between them is illustrated in Fig. 9 for two cases: (i) it is assumed that the displaced atom has to travel a minimum distance $2a$ (where a is the cube-cell side) in the ⟨100⟩ direction before coming to rest as a stable interstitial; (ii) this minimum distance is assumed to be $3a$. The underlined numbers on Fig. 9 give the minimum energy which is required to obtain a separation distance between interstitial and vacancy larger than the minimum one, i.e., $\geq 3a$ in case (i) and $\geq 4a$ in case (ii). This energy is to be compared with $T_{d2}^{\langle 100\rangle}$ in model II. The other numbers on Fig. 9 give the energy which is required to induce 5, in case (i), or 7, in case (ii), replacements in the ⟨111⟩ direction. This energy is to be compared to the threshold energy $T_d^{\langle 111\rangle}$. The framed numbers indicate, in each case, the amount of energy lost per replacement. It is seen that most of the energy required to induce a ⟨111⟩ displacement is used to build up the "compressed configuration" which is then propagated along ⟨111⟩ without notable energy loss. Our best choice for the interatomic potential will lie in the range between $V(r) = 61\,000e^{-4.5r}$ and $V(r) = 485\,000e^{-5.5r}$, V being expressed in eV and r in Å. This potential is compared on Fig. 10 to the one proposed by Andersen and Sigmund,[25] $V_{AS}(r)$

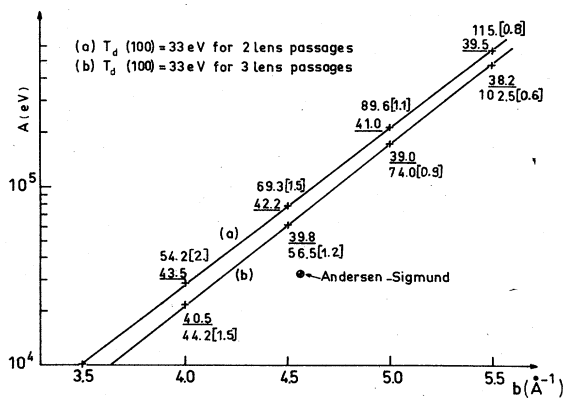

FIG. 9. Relations between the Born-Mayer potential constants A and b, so as to yield $T_{d1}^{\langle 100\rangle} = 33$ eV either after two (curve a) or after three (curve b) lens passages in the ⟨100⟩ direction. For each pair (A, b) is given the threshold energy $T_{d2}^{\langle 100\rangle}$ (underlined number) and the threshold energy $T_d^{\langle 111\rangle}$ for five (case a) or seven (case b) lens passages in the ⟨111⟩ direction.

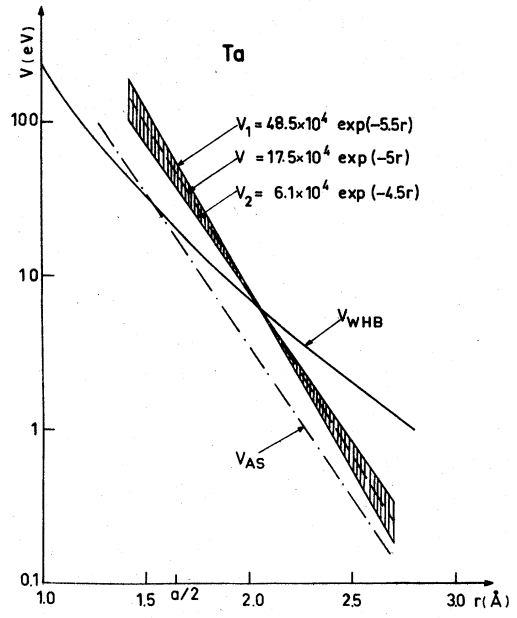

FIG. 10. Various interatomic potentials for tantalum. Potentials V_1, V, and V_2 are taken out of Fig. 9.

$= 32\,000e^{-4.56r}$, and to that deduced from recent work by Wilson *et al.*[26] giving a universal average potential for the calculation of ranges and stopping power of low-energy projectiles ($\gtrsim$1 eV).

D. Stage-I recovery

Previous studies of the recovery spectrum of tantalum after electron irradiation at helium temperatures[13,17,27] have shown that stage I takes place below 20 K. The free interstitial migration has been commonly assumed to occur around 17.5 K, its correlated recovery being attributed to the most important peak centered at 14 K. However, this interpretation has been recently questioned by Dausinger *et al*,[28] whose results point to free migration at $T \lesssim 17$ K and even allow free migration to take place below 4.5 K, this latter assumption giving a more straightforward explanation of the important suppression of stage I by doped-in oxygen concentrations of as low as 100 ppm.

Three isochronal anneals ($\Delta t = 10$ min) were performed after irradiations at 1.0, 1.3, and 1.7 MeV (cf. Table III). A slow and continuous anneal was observed between 7 and 35 K; stage I was almost nonexistent, even at 1.7 MeV, which concurs with what is known of the strong influence of the impurities.

The experimental amplitude of stage I at 1.7 MeV has been compared to values deduced from the cross sections calculated with model II. For this comparison, it has been assumed that the subthreshold defect production was unchanged from 1.0 to 1.7 MeV, and the resistivity variations measured at 1.0 MeV have been subtracted from those measured at 1.7 MeV, for equal fluences. The corresponding values are listed in Table IV, together with the calculated percentages of defects which are produced, in model II, with a transmitted energy T lying between 33 and 38 eV. As a matter of fact, it is a quite straightforward assumption to suppose that at least those pairs which are the nearest ones will give rise to close-pair recombination. Now it can be seen from Table IV that the experimental values for the normalized stage-I amplitude are much lower than the calculated ones, leading to the assumption that even the closest pairs produced in the ⟨100⟩ direction will not give rise to close-pair recombination but rather annihilate through correlated or free interstitial migration. This would explain why stage I is so strongly suppressed by the presence of impurities, in concentrations even as low as 10^{-4}.

TABLE IV. Percentages of intrinsic defects recovering during stage I compared to calculated values.

	(100)	(112)	(110)	(111)
$\frac{100[\Delta\rho_{ann}^{21K}(1.7)-\Delta\rho_{ann}^{21K}(1.0)]}{\Delta\rho_{irr}(1.7)-\Delta\rho_{irr}(1.0)}$	9±7 ?	2±2	10±8	5±5
% of close pairs calc. with model II	13	26	30	24
% of defects produced through region II calc. with model I	61	47	48	44

Let us note finally that model I cannot allow any interpretation of the recovery results, since it leads at 1.7 MeV to a nearly equal production of defects through region I and region II as can be seen in Table IV; none of the two corresponding mechanisms can, therefore, be directly related to close-pair production.

V. CONCLUSIONS

The experimental data obtained in the present work show definitely that, contrary to Jung and Schilling's results, but, similar to all other already studied bcc metals, the easiest atomic displacements in Ta take place in and around the ⟨100⟩ direction, the corresponding threshold energy being $T_d^{\langle 100\rangle} = 33 \pm 1$ eV.

If we then remember that a Frenkel pair produced along a ⟨100⟩ direction in a bcc crystal can end up in two different configurations regarding the interaction between interstitial and vacancy, the most straightforward explanation of the present results leads us to assume that, for the closest

pairs, one of these two configurations is unstable at the irradiation temperature (7 K).

Finally, we suggest, as a possible explanation for the extreme impurity sensitivity of the observed stage-I recovery, that the closest ⟨100⟩ pairs which are stable at the irradiation temperature may not undergo close-pair recombination but rather correlated recombination through long-range interstitial migration.

ACKNOWLEDGMENTS

The excellent technical assistance of the accelerator team is greatly appreciated. Thanks are due to Dr. Biscondi, Ecole des Mines de St. Etienne, who provided us the single-crystal rods. We are grateful to Dr. M. L. Swanson of the Chalk River Nuclear Labs., Chalk River, Canada, for the backscattering analysis of the irradiated specimens.

---

*Laboratoire de Physique de l'Ecole Normale Supérieure de Jeunes Filles, F-92120, Montrouge, France.

[1]P. Jung and W. Schilling, Phys. Rev. B 5, 2046 (1972).
[2]C. Erginsoy, G. H. Vineyard, and A. Englert, Phys. Rev. 133, A595 (1964).
[3]J. N. Lomer and M. Pepper, Philos. Mag. 16, 1119 (1967).
[4]M. Biget, P. Vajda, A. Lucasson, and P. Lucasson, Radiat. Eff. 21, 229 (1974).
[5]F. Maury, P. Vajda, M. Biget, A. Lucasson, and P. Lucasson, Radiat. Eff. 25, 175 (1975).
[6]F. Maury, M. Biget, P. Vajda, A. Lucasson, and P. Lucasson, Phys. Rev. B 14, 5303 (1976).
[7]F. Dausinger, Ph.D. thesis (University of Stuttgart, 1975) (unpublished).
[8]P. Vajda, Rev. Mod. Phys. 49, 481 (1977).
[9]M. Biget and P. Vajda, J. Phys. E 6, 968 (1973).
[10]W. J. McG. Tegart, *The Electrolytic and Chemical Polishing of Metals* (Pergamon, New York, 1959).
[11]A. Lucasson, P. Lucasson, and G. Lelogeais, Cryogenics 6, 169 (1966).
[12]D. Meissner and W. Schilling, Z. Naturforsch. 26, 502 (1971).
[13]K. H. Faber, Ph.D. thesis (University of Stuttgart, 1973) (unpublished).
[14]F. Maury, P. Vajda, A. Lucasson, and P. Lucasson, Radiat. Eff. 10, 239 (1971).
[15]F. Maury, P. Vajda, A. Lucasson, and P. Lucasson, Phys. Rev. B 8, 5496 (1973).
[16]K. Rosan and H. Wipf, Phys. Status Solidi A 38, 611 (1976).
[17]J. N. Daou, J. E. Bonnet, P. Vajda, M. Biget, A. Lucasson, and P. Lucasson, Phys. Status Solidi A 40, 101 (1977).
[18]J. Schweikhardt, Diplomarbeit (University of Stuttgart, 1975) (unpublished).
[19]P. Jung, Kernforschungsanlage Jülich Report No. Jül.-729-FF (Jülich, Germany, 1971) (unpublished).
[20]G. Youngblood, S. Myhra, and J. W. de Ford, Phys. Rev. 188, 1101 (1969).
[21]O. S. Oen, Oak Ridge Natl. Lab. Rept. No. ORNL-4897, 1973 (unpublished).
[22]F. Maury and P. Lucasson, Phys. Status Solidi A 34, 513 (1976).
[23]W. Dönitz, W. Hertz, W. Waidelich, H. Peisl, and K. Böning, Phys. Status Solidi A 22, 501 (1974).
[24]F. Maury, P. Vajda, A. Lucasson, and P. Lucasson, Phys. Rev. B 8, 5506 (1973).
[25]H. H. Andersen and P. Sigmund, Danish AEC Risö Report No. 103, 1965 (unpublished).
[26]W. D. Wilson, L. G. Haggmark and J. P. Biersack, Phys. Rev. B 15, 2458 (1977).
[27]H. Hemmerich, D. Meissner, H. Schultz, and F. Walz, in Proceedings of the Conference on Vacancies and Interstitials in Metals, Jülich, 1968, p. 724 (unpublished).
[28]F. Dausinger, J. Fuss, J. Schweikhardt, and H. Schultz, International Conference on the Properties of Atomic Defects in Metals, Argonne, 1976 (unpublished).